Single crystal structure and photocatalytic behavior of grafted uranyl on the Zr-node of a pyrene-based metal-organic framework

Journal:	*CrystEngComm*
Manuscript ID	CE-ART-12-2019-002034.R1
Article Type:	Paper
Date Submitted by the Author:	19-Feb-2020
Complete List of Authors:	Knapp, Julia; Northwestern University, Chemistry Zhang, Xuan; Northwestern University, Elkin, Tatyana; Los Alamos National Laboratory Wolfsberg, Laura; Los Alamos National Laboratory Hanna, Sylvia; Northwestern University, Chemistry Son, Florencia; Northwestern University, Department of Chemistry Scott, Brian; Los Alamos National Laboratory, Materials Physics and Applications Farha, Omar; Northwestern University, Department of Chemistry

SCHOLARONE™
Manuscripts

Single crystal structure and photocatalytic behavior of grafted uranyl on the Zr-node of a pyrene-based metal-organic framework

Julia G. Knapp,[a] Xuan Zhang,[a] Tatyana Elkin,[d] Laura E. Wolfsberg,[c] Sylvia L. Hanna,[a] Florencia A. Son,[a] Brian L. Scott*,[d] Omar K. Farha*[a,b,e]

Department of Chemistry, Northwestern University, 2145 Sheridan Road, Evanston, Illinois 60208, United States

International Institute for Nanotechnology, Northwestern University, 2145 Sheridan Road, Evanston, Illinois 60208, United States

Inorganic, Isotope and Actinide Chemistry (C-IIAC), Los Alamos National Laboratory, Los Alamos, NM, 87545, USA

Materials Synthesis and Integrated Devices (MPA-11), Los Alamos National Laboratory, Los Alamos, NM, 87545, USA

Department of Chemical and Biological Engineering, Northwestern University, 2145 Sheridan Road, Evanston, Illinois 60208-3113, United States

Abstract

Accurately characterizing actinide oxides bound to metal–organic frameworks (MOFs) is important for designing MOFs as radioactive waste sorbents and catalytic supports. In this work, the zirconium MOF NU-1000 was post-synthetically modified through solvothermal deposition to include the uranyl (UO_2^{2+}) ion and characterized *via* single-crystal X-ray diffraction. Bond lengths derived from the diffraction pattern and Raman spectroscopy indicate that UO_2^{2+} maintains its chemical properties upon deposition, while alcohol oxidation photocatalysis reveals photo-interactions between the pyrene linkers and the UO_2^{2+} ion.

Introduction

Metal–organic frameworks (MOFs) are porous, crystalline solids with extended structures that self-assemble from tunable inorganic nodes and organic linkers.[1-4] Zirconium-based MOFs (Zr-MOFs) exhibit a diversity of topologies, along with high chemical and thermal stability and often scalable syntheses.[5-8] A common Zr node structure is the $[Zr_6(\mu_3\text{-}O)_4(\mu_3\text{-}OH)_4]^{12+}$ cluster, which may be 4-, 6-, 8-, 9-, 10-, or 12-connected depending on the choice of polytopic carboxylate-based ligand.[9-13] Should the cluster be connectively unsaturated (<12 metal-ligand bonds), terminal aqua and hydroxyl groups bound to Zr(IV) balance the charge; these groups are capable of binding additional guests through ion exchange and coordination.[14] The atomically precise binding motifs of the metal ions can be elucidated through single-crystal X-ray diffraction (SCXRD).[15, 16] Successful installation of metal ions onto Zr-MOF nodes has been achieved through atomic-layer deposition and solvothermal deposition.[17]. Because the metal-oxo bonds formed at these terminal sites are quite strong, they allow for quick capture of metal ions and are thus relevant to heavy metal remediation. For example, several toxic compounds, including SeO_4^-,[14] ReO_4^-,[18] and As(V)[19] are captured by binding to Zr nodes with equilibration times of less than 12 hours. Additionally, strong metal-oxo bonds at Zr-MOF nodes are also relevant to heterogeneous, single site catalysis. Our group and others have shown that Zr-MOFs can support transition metal ions and oxides as catalysts for ethylene dimerization[20] and alcohol oxidation,[21] while still maintaining the innate stability and crystallinity of the Zr-MOF.

However, there are far fewer examples of actinide ions, such as uranium, bound to Zr-MOF nodes as compared to transition metal binding.[22] The uptake and grafting of uranium is important for water treatment,[23] since the uranyl ion, a doubly charged species where uranium is bound to two axial oxygen atoms (UO_2^{2+}), is frequently observed at node and linker sites.[24, 25] Additionally, the uranyl ion has shown promise as a photocatalyst within the homogeneous phase, due to its long-lived excitation state and strong oxidizing potential,[26] exhibiting versatile reactivity for alkane fluorination,[27] alcohol oxidation,[28] and alkane oxidation reactions.[29] When incorporated into crystalline zeolites, UO_2^{2+} demonstrates improved oxidation of isopropanol to acetone.[30] Thus, we speculate that grafting UO_2^{2+} in a crystallographically identifiable manner onto a hierarchical MOF may increase the rate of catalytic reactions while providing support against over-oxidation to the immobile solid uranium dioxide (UO_2). Furthermore, elucidating uranyl binding motifs from atomically precise crystal structures will aid in designing improved sorbents for uranyl uptake and uranium-based photocatalysis with higher quantum efficiency.[31,32]

Herein, we report the synthesis of the Zr-MOF, NU-1000, with UO_2^{2+} grafted on its node **(NU-1000-U)** *via* solvothermal deposition and its activity as a photocatalyst for the oxidation of 4-methoxybenzyl alcohol under visible light irradiation. We chose NU-1000 due to combination of structurally and chemically vital features, such as high porosity, hierarchical structure, chemical and thermal stability, and coordinatively unsaturated 8-connected Zr_6 cluster.[33] The H_4TBAPy linkers are also photoactive, providing an opportunity to investigate how MOF photocatalysis proceeds in the presence of two potential active sites (grafted uranyl and H_4TBAPy linker) and to identify structure-activity relationships beyond node-linker interactions.[34, 35] This study is the first of its kind to report the single-crystal structure of an actinide ion adsorbed onto a MOF.

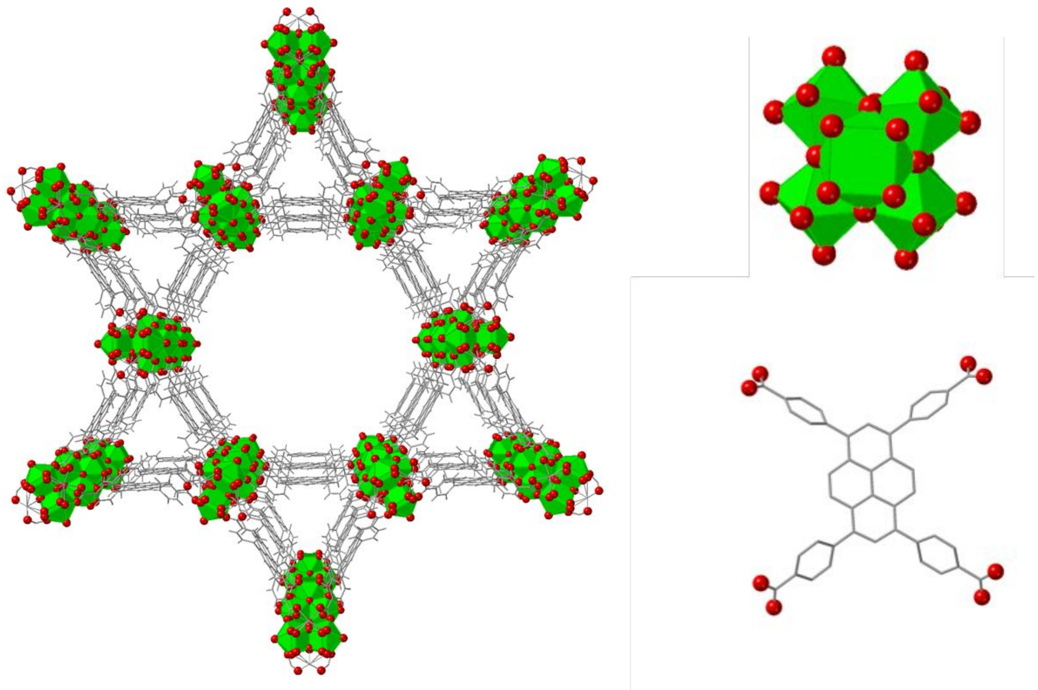

Figure 1. NU-1000 MOF (left) with Zr_6 nodes (top right) and carboxylic acid linkers (bottom right) (Zr = green polyhedra, O = red dots, C = gray rods). Hydrogen atoms excluded for clarity.

Results and Discussion

NU-1000-U was synthesized *via* solvothermal deposition of uranyl acetate onto NU-1000, and its presence in the MOF was confirmed by multiple characterization methods. Crystallinity was maintained after solvothermal deposition, as confirmed by PXRD (Fig. 2A). The loading of UO_2^{2+} was approximately 1.3 per node, calculated by inductively coupled plasma optical emission spectroscopy. Scanning electron microscopy and energy dispersive x-ray spectroscopy analysis indicate presence of uranium throughout the entire length of the particle (Fig. S1). Diffuse reflectance Fourier transform spectroscopy also confirms the presence of UO_2^{2+} with a slight change in the shape of the terminal hydroxyl peaks (3667 cm^{-1}) and the appearance of a peak at 918 cm^{-1} after UO_2^{2+} grafting (Fig. 2B). This antisymmetric uranium-oxo stretching vibration is red-shifted from the stretching vibration of hydrated UO_2^{2+} (963 cm^{-1}) and has previously been assigned to UO_2^{2+} oxo-binding and a subsequent loss of coordinated solvent.[36] Thermogravimetric analysis indicated removal of water, but it is unclear whether this water was coordinated to uranium or within the pores (Fig. S2). To determine if acetate from uranyl acetate dihydrate interacts with the Zr_6 node during deposition, **NU-1000-U** was dissolved in base and ^1H NMR spectra were collected; approximately 1 acetate moiety per Zr_6 node was calculated (Fig. S3). Importantly, N_2 isotherms collected at 77K demonstrate a surface area of 2200 m^2/g for NU-1000 and 1980 m^2/g (Fig. 2C) for **NU-1000-U** with negligible change to the overall pore size (Fig. 2D).

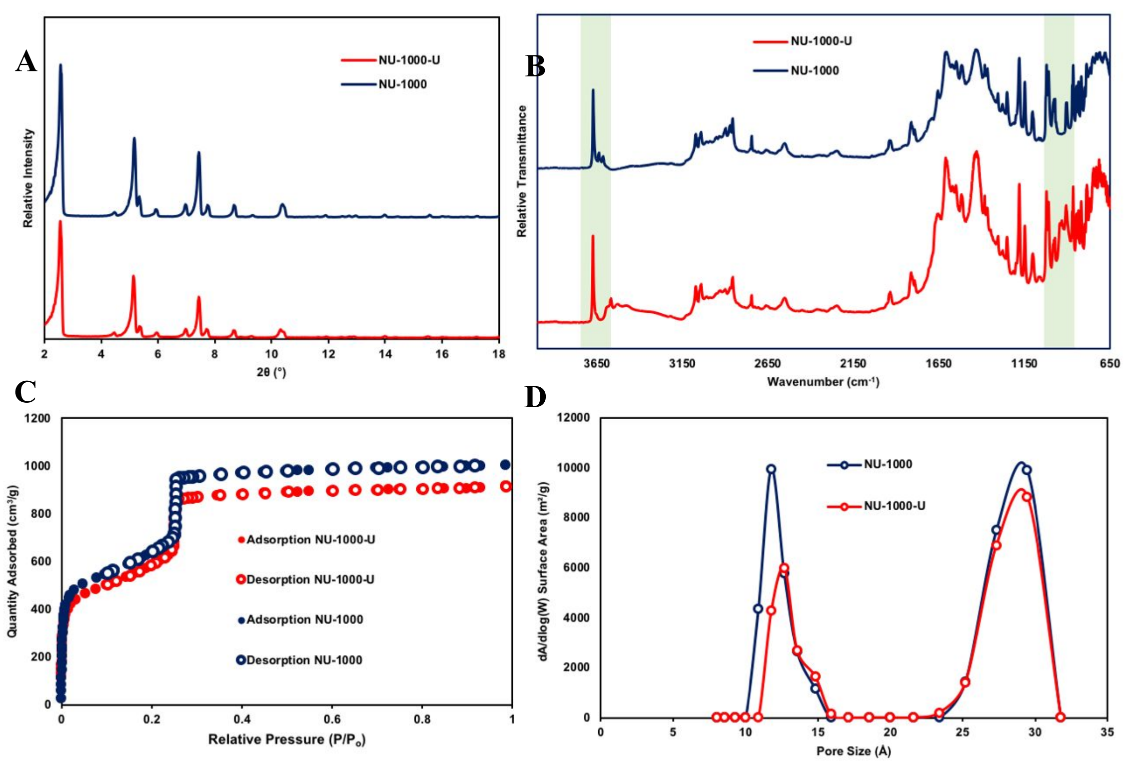

Figure 2. Characterization for NU-1000 (blue) and NU-1000-U (red). A) PXRD patterns of activated NU-1000 and **NU-1000-U,** B) DRIFTS spectra, with peaks at 3667 (terminal hydroxyl)

and 918 cm^{-1} (loss of coordinated solvent) highlighted in blue, C) N_2 isotherms, and D) Pore size distributions.

To precisely determine the position of UO_2^{2+} within the framework, single crystals of **NU-1000-U** were synthesized, and SCXRD studies were performed. **NU-1000-U** is in the *P6/mmm* space group, with unit cell parameters of *a* = 39.5261 Å, *b* = 39.5261 Å, and *c* = 16.5278 Å. As compared to the crystal structure of pristine NU-1000 (*a* = 39.2976 Å, *b* = 39.2672 Å, *c* = 16.5666 Å), there is a 1.07% increase in cell volume. The changes in the *a* and *b* axes are attributed to shifts in the linker position to accommodate the large size of uranium. UO_2^{2+} binds in a bidentate fashion to the node (Fig. 5) and is not selective towards binding in the mesopore or micropore (Fig. 2a), in agreement with the N_2 isotherm. The uranium atoms occur in two crystallographically independent positions at each binding site. As a consequence of disorder, the oxygens of the uranyl unit are not visible within the crystal structure. The oxygen atoms bound to uranium are most likely additional hydroxyl or aqua groups, consistent with TGA data. **NU-1000-U** also has slightly shortened Zr-μ_3O bond lengths relative to both NU-1000 and other published metal-loaded NU-1000 SIM structures, indicating potential interactions between UO_2^{2+} and the Zr_6 node (Table 1).[20, 31, 33, 37-39]

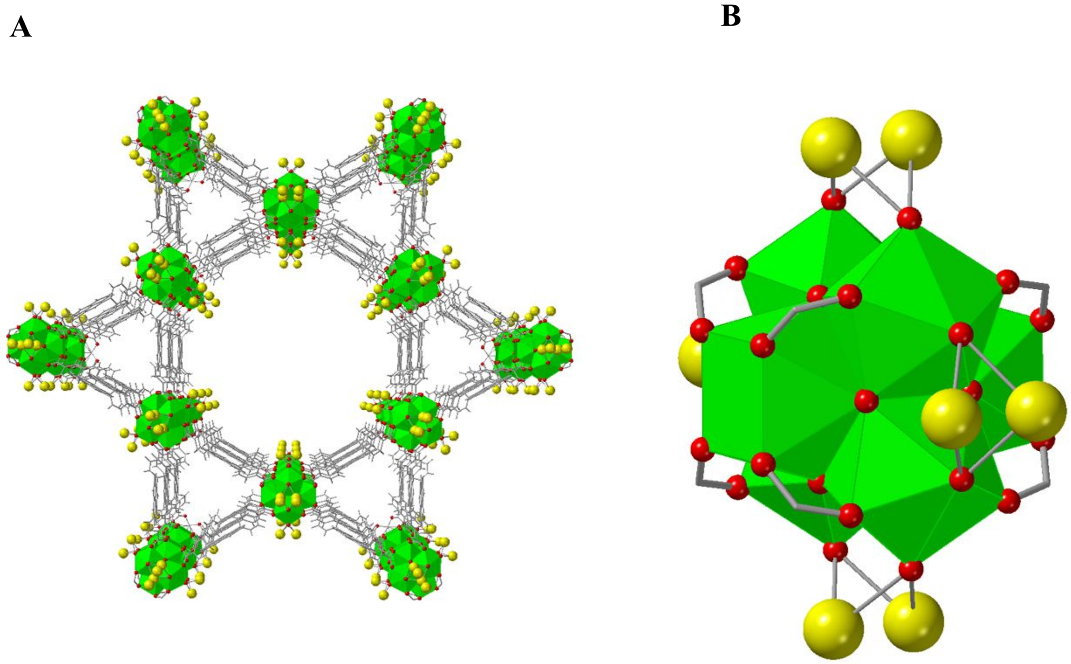

Figure 3. A) NU-1000-U full structure demonstrating the two crystallographically equivalent positions. Uranium is represented in yellow. B) Close-up image of Zr_6 node with grafted uranyl (linker binding sites in gray).

Table 1. Average bond lengths between Zr^{4+} and -μ_3O moieties in selected NU-1000 SIM derivatives.

MOF	Average Zr-μ_3O Bond Length (Å)	Ref. Number
NU-1000	2.141	33
NU-1000-U	2.075	This work
MoOx-SIM	2.166	31
MoSx-SIM	2.156	37
NU-1000-Cr	2.162	20
NU-1000-Re	2.159	38
NU-1000-V	2.171	39

Thus, Raman spectroscopy was implemented to characterize the axial U-O bond lengths. The U-O bond length may be assessed by the modified Badger's equation, which relates the vibrational spectroscopic properties of the $[UO_2]^{2+}$ cation to the crystallographic bond length with an average of 3 pm accuracy.[40] The symmetric stretch of $[UO_2]^{2+}$ in pure uranyl acetate was observed at 856 cm^{-1}, which is consistent with the previously reported literature.[40] **NU-1000-U** exhibits two signals: one at the same wavenumber as pure uranyl acetate (856 cm^{-1}) and one at 851 cm^{-1} (Fig. 4). The 856 cm^{-1} peak could indicate that the acetate ligand seen in the ^{1}H NMR remains coordinated to $[UO_2]^{2+}$ upon deposition. The 851 cm^{-1} peak likely corresponds to vibrations of the bonds between $[UO_2]^{2+}$ and the terminal hydroxyl groups of the Zr_6 node, upon comparison to the similar complex $(UO_2)_2(OH)_2$ (853 cm^{-1})[41] and other uranyl-hydroxyl species.[42] Using Badger's equation, the estimated bond lengths of the $[UO_2]^{2+}$ species observed in **NU-1000-U** are 1.75 $\pm$ 0.03 Å and 1.76 $\pm$ 0.03 Å for 856 cm^{-1} and 851 cm^{-1}, respectively. This suggests that the uranyl-oxo bonds do not change significantly upon deposition.

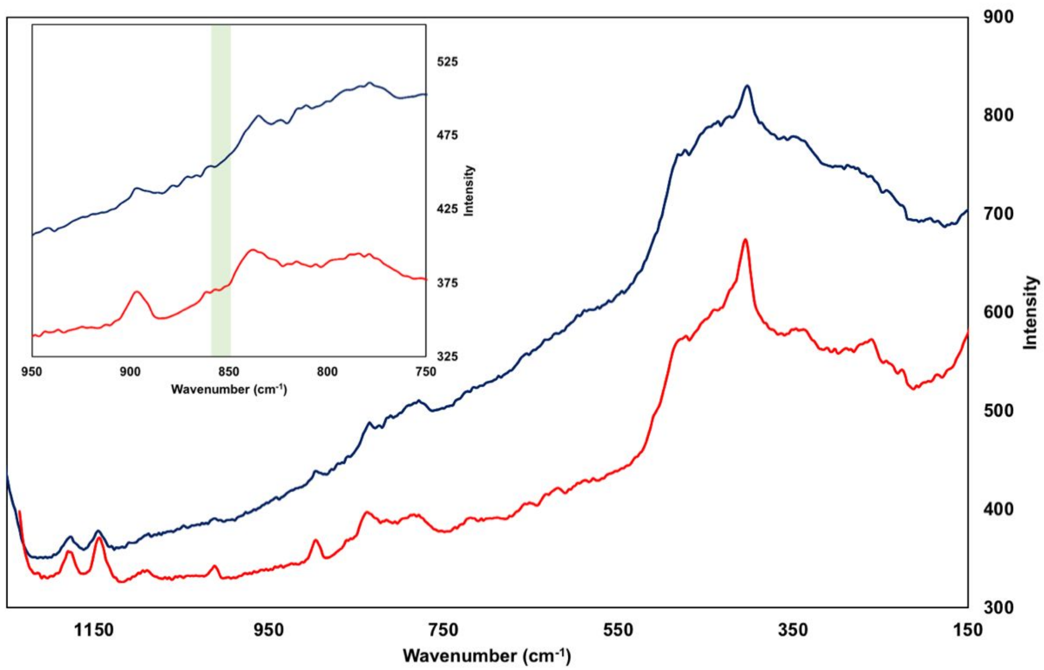

Figure 4: Raman spectra of **NU-1000** (top, blue) and **NU-1000-U** (bottom, red) with peaks at 851 cm^{-1} and 856 cm^{-1} in NU-1000-U highlighted in green within insert.

Because the photocatalytically active uranyl ion was successfully grafted to the Zr node, photocatalysis experiments were performed to determine whether the presence of a photo-active linker within a stable framework would interfere with uranyl photocatalysis. Alcohol oxidation experiments (Fig. 5A) were run under blue light in an O_2 atmosphere with 5% catalyst loading; conversion was tested for powder NU-1000, NU-1000-U, and uranyl acetate dihydrate, as a control (Fig. 5B). NU-1000 displayed the highest conversion (40%, after 24 hours), followed by uranyl acetate (22%, after 28 hours), and NU-1000-U (12% after 24 hours). The conversions indicate that when both H_4TBAPy and UO_2^{2+} are present, the rate of reaction decreases, likely from photo-interactions between UO_2^{2+} and the H_4TBAPy linker (see supporting information for further discussion). Control experiments were also implemented using the photo-inactive Zr-MOF NU-1200, which has same node structure and connectivity of NU-1000 (2% conversion after 24 hours). This low conversion of NU-1200 demonstrates that the H_4TBAPy linker, rather than the Zr_6 node, is the active site for photocatalysis in NU-1000. Finally, photocatalytic conversion of a mixture of uranyl acetate and H_4TBAPy was examined (9% conversion after 24 hours). Since this conversion is lower than that of uranyl acetate alone, it suggests that the uranyl excited state is quenched by the exciplexes produced by the excited pyrene linker, and vice versa (Table S2). These results are a proof-of-concept that photo-active linkers of a MOF interact with photo-active grafted metals and may introduce a new method of altering the electronics of uranyl photochemically to stabilize unusual oxidation states, such as U(V).

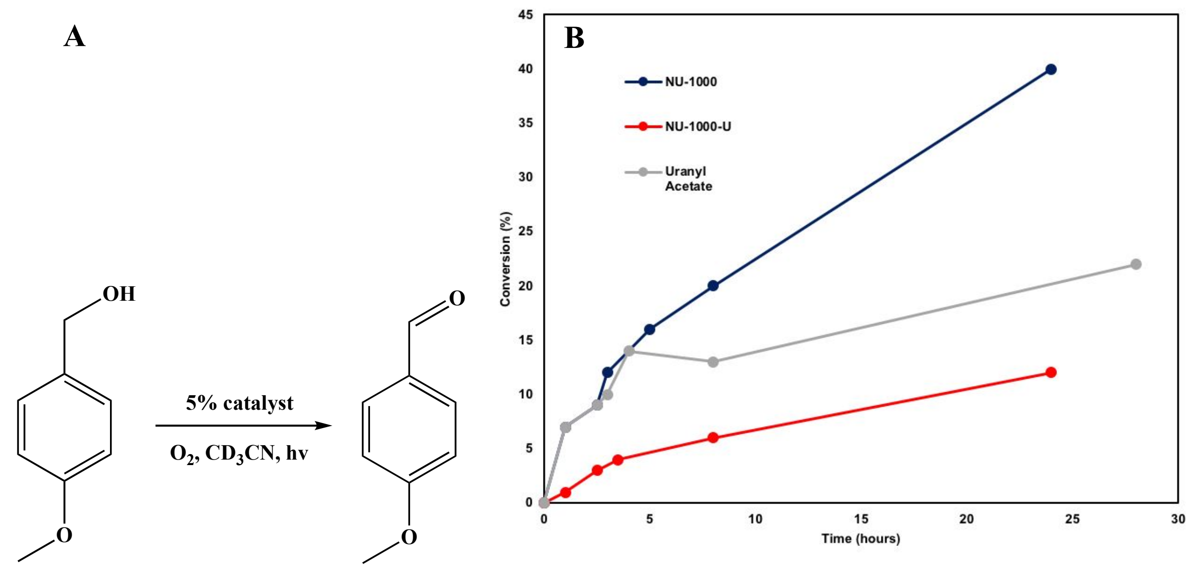

Figure 5. a) Reaction scheme for oxidation of 4-methoxybenzyl alcohol and b) kinetics plot of NU-1000, NU-1000-U, and the uranyl ion for 4-methoxybenzyl alcohol oxidation.

Conclusion

The uranyl-loaded framework **NU-1000-U** was synthesized via solvothermal deposition of uranyl acetate onto NU-1000 and characterized in powder and single crystal phases. This single-crystal structure is the first report of an actinide ion grafted onto a Zr-based MOF, and it reveals slightly shortened Zr-μ_3O bonds which corresponds to potential interactions between UO_2^{2+} and the Zr_6 node. The reduced photocatalytic activity in the oxidation of 4-methoxybenzyl alcohol of **NU-1000-U** relative to either NU-1000 or the uranyl ion alone indicates interactions between the H_4TBAPy linker and uranyl, which may be an important consideration when developing new MOF supports.

ASSOCIATED CONTENT

Supporting Information

Crystallographic data for **NU-1000-U** (CIF)

Materials, synthesis, and characterization, crystallographic data for **NU-1000-U**, TGA curves, SEM images and EDX mapping, proton NMR spectra.

AUTHOR INFORMATION

Corresponding Authors

* E-mail: bscott@lanl.gov

* E-mail: o-farha@northwestern.edu

Notes

The authors declare no competing financial interest.

ACKNOWLEDGMENT

O.K.F. acknowledges the support from the U.S. Department of Energy, National Nuclear Security Administration, under Award Number DE-NA0003763. The authors acknowledge the Integrated Molecular Structure Education and Research Center (IMSERC) at Northwestern University, which has received support from the National Science Foundation (NSF grants CHE-1048773 and DMR-0521267). We also acknowledge the Soft and Hybrid Nanotechnology Experimental (SHyNE) Resource (NSF NNCI-1542205) and the International Institute for Nanotechnology (IIN). We also acknowledge the Quantitative Bio-element Imaging Center (QBIC).

References

1. Zhou, H. C., Long, J., Yaghi, O. M., *Chem. Rev.* **2012,** *112* (2), 673-674.
2. Kitagawa, S., Kitaura, R., Noro, S., *Angew. Chem. Int. Ed.* **2004,** *43* (18), 2334 - 2375.
3. Li, H., Eddaoudi, M.,O'Keeffe, M., Yaghi, O. M. , *Nature* **1999,** *402*, 276 - 279.
4. Rosi, N. L., Eddaoudi, M., Kim, J., O'Keeffe, M., Yaghi O.M., *CrystEngComm.* **2002,** *4*, 401 - 404.
5. Bai, Y., Dou, Y., Xie, L.H., Rutledge, W., Li, J.R., Zhou, H.C., *Chem. Rev.* **2016,** *45*, 2327-2367.

6. Howarth, A. J., Liu, Y., Li, P., Li, Z., Wang, T. C., Hupp, J. T., Farha, O. K., *Nat. Rev. Mater.* **2016,** *1*, 15108 - 15032.

7. Užarević, K., Wang, T.C., Moon, S.Y., Fidelli, A.M., Hupp, J.T., Farha, O.K., Friščić, T., *Chem. Comm.* **2016,** *52*, 2133 - 2136.

8. Karadeniz, B., Howarth, A.J., Stolar, T., Islamoglu, T., Deganović, I., Tireli, M., Wasson, M.C., Moon, S.Y., Farha, O.K., Friščić, T., Užarević, K., *ACS Sustainable Chem. Eng.* **2018,** *6*, 15841 - 15849.

9. Chen, Y., Zhang, X., Ma, K., Chen, Z., Wang, X., Knapp, J., Alayoglu, S., Wang, F., Xia, Q., Li, Z., Islamoglu, T., Farha O.K., *ACS Appl. Nano Mater.* **2019,** *2* (10), 6098-6102.

10. Jiang, H. L., Feng, D., Wang, K., Gu, Z.Y., Wei, Z., Chen Y.P., Zhou, H.C. , *J. Am. Chem. Soc.* **2013,** *135*, 13934 —13938.

11. Feng, D., Chung, W.C., Wei, Z., Gu, Z.-Y., Jiang, H.L., Chen, Y.P., Darensbourg, D.J., Zhou, H.C., *J. Am. Chem. Soc.* **2013,** *135*, 17105 - 17110.

12. Liang, W., Chevreau, H., Ragon, F., Southon, P. D., Peterson, V. K., D'Alessandro, D. M., *CrystEngComm* **2014,** *16*, 6530 - 6533.

13. Zhang, Y., Zhang, X., Lyu, J., Otake, K., Wang, X., Redfern, L.R., Malliakas, C.D., Li, Z., Islamoglu, T., Wang, B., Farha, O.K., *J. Am. Chem. Soc.* **2018,** *140*, 11179 - 11183.

14. Howarth, A. J., Katz, M. J., Wang, T. C., Platero-Prats, A. E., Chapman, K. W., Hupp, J.T., Farha, O.K., *J. Am. Chem. Soc.* **2015,** *137*, 7488 - 7494.

15. Vermoortele, F., Vandichel, M., Van de Voorde, B., Ameloot, R., Waroquier, M., Van Speybroeck, V., De Vos, D. E., *Angew. Chem. Int. Ed.* **2012,** *51*, 4887-4890.

16. Yuan, S., Chen, Y. P., Qin, J. S., Lu, W. G., Wang, X., Zhang, Q., Bosch, M., Liu, T. F., Lian, X. Z., Zhou, H. C., *Angew. Chem., Int. Ed.* **2015,** *54*, 14696 – 14700.

17. Islamoglu, T., Goswami, S., Li, Z., Howarth, A. J., Farha, O. K., Hupp, J. T., *Acc. Chem. Res.* **2017,** *50*, 805 - 813.

18. Banerjee, D., Xu, W., Nie, Z., Johnson, L. E., Coghlan, C., Sushko, M. L., Kim, D., Schweiger, M. J., Kruger, A. A., Doonan, C. J. , *Inorg. Chem.* **2016,** (55), 8241 - 8243.

19. Li, Z., Yang, J., Sui, K., Yin, N., *Mater. Lett.* **2015,** *160*, 412 - 414.

20. Goetjen, T. A., Zhang, X., Liu, J., Hupp, J.T., Farha, O.K., *ACS Sustainable Chem. Eng.* **2019,** (7), 2553 - 2557.

21. Wang, W., Zhang, X., Li, P., Otake, K., Cui, Y., Lyu, J., Kryzaniak, M.D., Buru, C.T., Islamoglu, T., Wasielewski, M.R., Li, Z., Farha, O.K., *J. Am. Chem. Soc.* **2019,** *141*, 8306 - 8314.

22. Chen, L., Bai, Z., Zhu, L., Zhang, L., Cai, Y., Li, Y., Liu, W., Wang, Y., Chen, L., Diwu, J., Wang, J., Chai, Z., Wang, S., *ACS Appl. Mater. Interfaces* **2017,** *9*, 32446 - 32451.

23. Zhang, T., Ling, B.K., Hu, Y.Q., Han, T., Zheng, Y.Z., *CrystEngComm.* **2019,** *21*, 3901 - 3905.

24. Berseneva, A. A., Martin, C.R., Galitskiy, V.A., Ejegbavwo, O.A., Leith, G.A., Ly, R.T., A.M. Rice, Dolgopolova, E. A., Smith, M.D., zur Loye, H.C., DiPrete, D.P., Amoroso, J.W., Shustova, N.B., *Inorg. Chem.* **2019**.

25. Pandey, S., Jia, Z., Demaske, B., Ejegbavwo, O. A., Setyawan, W., Henager, C. H., Shustova, N. B., Phillpot, S. R., *J. Phys. Chem. C* **2019,** *123*, 26842 - 26855.

26. Balzani, V., Bolletta, F., Ganfoldi, M. T., Maestri M. , *Top. Curr. Chem.* **1978,** *75*, 1.

27. West, J. G., Bedell, T. A., Sorenson, E. J., *Angew. Chem., Int. Ed.* **2016,** *55*, 8923 - 8927.

28. Li, Y., Su, J., Mitchell, E., Zhang, G.Q., Li, J., *Sci. China Chem.* **2013,** *56*, 1671 - 1678.

29. Wang, W. D., Bakac, A., Espenson, J.H., *Inorg. Chem.* **1995,** *34*, 6034 - 6039.

30. Sui, S. L., Kostapapas, A., Psaras, D., *J. Am. Chem. Soc.* **1984,** *106*, 1614 - 1620.

31. Noh, H., Cui, Y., Peters, A.W., Pahls, D.R., Ortuno, M.A., Vermeulen, N.A., Cramer, C.J., Gagliardi, L., Hupp, J.T., Farha, O.K. , *J. Am. Chem. Soc.* **2016,** *138*, 14720 - 14726.

32. Wang, X. F., Chen, Y., Song, L.P., Fang, Z., Zhang, J., Shi, F., Lin, Y.W., Sun, Y., Zhang, Y.B., Rocha, J., *Angew. Chem., Int. Ed.* **2019,** *58*.

33. Islamoglu, T., Otake, K., Li, P., Buru, C.T., Peters, A.W., Akpinar, I., Garibay, S.J., Farha, O.K., *CrystEngComm.* **2018,** *20*, 5913 - 5918.

34. Sava Gallis, D. F., Butler, K.S., Rohwer, L.E.S., A.A. McBride, Vincent, G., Chong, C.V., Pearce, C.J., Luk, T.S., *CrystEngComm.* **2018,** *20*, 5919 - 5924.

35. Sava Gallis, D. F., Rohwer, L.E.S., Rodriguez, M.A., Nenoff, T.M., *Chem. Mater.* **2014,** *26*, 2943 - 2951.

36. Manos, M. J., Kanatzidis, M. G., *J. Am. Chem. Soc.* **2012,** *134*, 16441 - 16446.

37. Noh, H., Kung, C.W., Otake, K., Peters, A. W., Li, Z., Liao, Y., Gong, X., Farha, O. K., Hupp, J.T., *ACS Catal.* **2018,** *8*, 9848 - 9858.

38. Drout, R. J., Otake, K., Howarth, A. J., Islamoglu, T., Zhu, L., Xiao, C., Wang, S., Farha, O.K., *Chem. Mater.* **2018,** *30*, 1277 - 1284.

39. Otake, K., Cui, Y., Buru, C. T., Li, Z., Hupp, J. T., Farha, O. K., *J. Am. Chem. Soc.* **2018,** *140*, 8652 - 8656.

40. Bartlett, J. R., Cooney, R.P., *J. Mol. Struct.* **1989,** *193*, 295 - 300.

41. Lu, G., Forbes, T.Z., Haes, A.J., *Anal. Chem.* **2016,** *88*, 773 - 780.

42. Basile, M., Unruh, D.K., Flores, E., Johns, A., Forbes, T.Z., *Dalton Trans.* **2015,** *44*, 2597 - 2605.

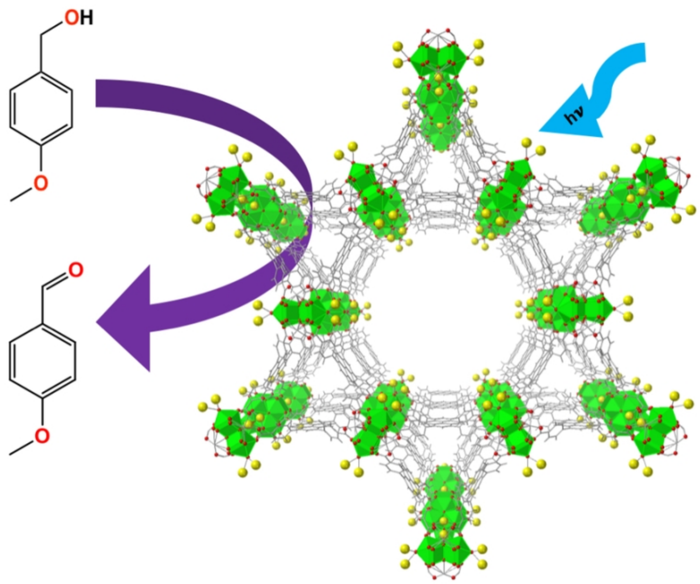

53x40mm (600 x 600 DPI)